

Source and a laser-heating system similar to one reported previously [C. S. Yoo *et al.*, *Phys. Rev. B* **48**, 15529 (1993)]. The x-ray beam size, 20  $\mu\text{m}$  by 20  $\mu\text{m}$ , was comparable to the size of laser-heating spot, which varied from 30 to 100  $\mu\text{m}$ , depending on the temperature. (For the later part of this study, we reduced the size of x-ray beam to 5  $\mu\text{m}$  by 20  $\mu\text{m}$  by focusing the 75  $\mu\text{m}$  by 20  $\mu\text{m}$  beam in the vertical direction with an x-ray focusing reflector.) Therefore, the temperature gradients could be large in both the radial and axial directions of the sample being x-rayed; we estimated that this could be as much as 10% of the value reported here. The x-ray diffraction of iron was collected at  $2\theta = 19^\circ$  or  $21^\circ$  for 1 to 10 min to obtain the spectra presented here. The microscope system contains an achromatic objective lens that can cause some chromatic aberration and, thereby, the uncertainty in temperature. This uncertainty could be significant in the case where the temperature is measured from a heating spot smaller than a few to several micrometers. However, considering the relatively large heating spot used in this study, we estimate that it is a minor effect. The details regarding the setup will be presented elsewhere [C. S. Yoo *et al.*, in preparation].

16. H. K. Mao *et al.*, *J. Appl. Phys.* **49**, 3276 (1978).
17. A. P. Jephcoat, R. J. Hemley, H. K. Mao, *Physica B* **150**, 115 (1988).
18. The  $d$  spacing of the new diffraction line, 2.229  $\text{\AA}$ , is close to the 100 peak of the NiAs structure of FeO found at 96 GPa and 800 K [Y. Fei and H.-K. Mao, *Science* **266**, 1678 (1994)], which could suggest that a new chemical reaction occurs at megabar pressures.
19. For example, the observed recrystallization of  $\epsilon$ -Fe at 2320 K (Fig. 2) is close to the previously reported  $\epsilon$ - $\beta$  boundary (5, 6). The change of texture could conceivably alter the nature of light reflection or absorption and give rise to the previously observed effect.
20. The  $\epsilon'$ -Fe phase was found at temperatures below those of  $\gamma$ -Fe and at pressures between 15 and 40 GPa. At 30 GPa, the volume of  $\epsilon'$ -Fe is about 6.111  $\text{cm}^3/\text{mol}$ , which lies between those of  $\epsilon$ -Fe (5.976  $\text{cm}^3/\text{mol}$ ) and  $\gamma$ -Fe (6.298  $\text{cm}^3/\text{mol}$ ) (C. S. Yoo *et al.*, in preparation).
21. S. K. Saxena *et al.*, *Science* **269**, 1703 (1995).
22. For convenience, we refer to the  $\gamma$ - $\epsilon$  phase line as the  $\gamma(\epsilon')$ - $\epsilon$  line. There are two constraints for the  $\gamma(\epsilon')$ - $\epsilon$  phase line. First, the resistivity measurements of iron at low pressures constrain the  $\gamma$ - $\epsilon$  phase line

below 20 GPa (13). Second, the present study shows that the  $\epsilon$ - $\gamma$ -liquid triple point is located at the vicinity of 50 GPa. To satisfy these two conditions, the  $\epsilon$ - $\gamma$  phase line cannot be concave down as presented in (5) and should be either concave up or at least straight. However, considering the existence of  $\epsilon'$ -Fe and the magnetic properties of  $\gamma$ -Fe and  $\epsilon'$ -Fe (20), the exact nature of the  $\gamma$ - $\epsilon$  phase line could be substantially more complicated.

23. We thank C. Ruddle and J. Hu for experimental assistance, B. Goodwin and C. Mailhot for support, and C. Meade, N. C. Holmes, W. J. Nellis, and M. Ross for discussions. Work at Lawrence Livermore National Laboratory (LLNL) was supported by the Laboratory Directed Research and Development Program grant LDRD 94-SR-042 and a Defense Program and was performed under the auspices of the U.S. Department of Energy (DOE) by LLNL under contract W-7405-ENG-48. Research at the Geophysical Lab and the National Synchrotron Light Source (NSLS) was supported by the National Science Foundation; NSLS is supported by DOE.

20 June 1995; accepted 25 August 1995

## Expansion of SN 1993J

J. M. Marcaide,\* A. Alberdi, E. Ros, P. Diamond, I. I. Shapiro, J. C. Guirado, D. L. Jones, T. P. Krichbaum, F. Mantovani, R. A. Preston, A. Rius, R. T. Schilizzi, C. Trigilio, A. R. Whitney, A. Witzel

A sequence of images from very long baseline interferometry shows that the young radio supernova SN 1993J is expanding with circular symmetry. However, the circularly symmetric images show emission asymmetries. A scenario in which freely expanding supernova ejecta shock mostly isotropic circumstellar material is strongly favored. The sequence of images constitutes the first "movie" of a radio supernova.

The recent discovery (1) by very long baseline interferometry (VLBI) of a shell-like radio structure in SN 1993J in the galaxy M81

offers the opportunity to monitor a supernova expansion in a manner that is free from modeling uncertainties (2, 3). Indeed, the angular resolution limit of VLBI, imposed by the size of the Earth, and the angular size of a supernova, determined by its distance from Earth, have generally not permitted a model-free determination of expansion in a young supernova. The relative proximity of SN 1993J, however, together with its strong centimeter emission, permit a reliable determination of the details of the expansion.

Our observations were carried out from September 1993 through September 1994 (Table 1). Images were obtained at 3.6 cm and 6 cm (Fig. 1). The image from November 1993 is from the discovery of the shell-like structure (1). The image from May 1994 was obtained with a large and well-calibrated array; therefore, all details in it are reliable. However, to obtain the images from September 1993 and February 1994, we used circularly symmetric models of sizes extrapolated and interpolated from the images from November 1993 and May 1994, respectively, as initial models in the mapping process. For the September 1993 image, extrapolation was needed because there was insufficient interferometric resolution to resolve the shell; and

for the February 1994 image, interpolation was needed because there were insufficient data (UV coverage) to reconstruct the image unambiguously without a priori information. The procedure we followed allowed us to reliably compare the sizes of the images obtained from the data at each epoch and thus to obtain the angular size growth rate and to learn how the emission enhancement in the southeastern part of the images evolved with time. The latter question is important in distinguishing which features of the emission correspond to traces of the initial explosion and which are induced by the dynamics of the evolution. In spite of the wavelength difference, the image at 6 cm (Fig. 1) from September 1994 shows a remarkably similar structure to those shown in images obtained at 3.6 cm at earlier epochs. However, comparison of the size of the image from this epoch with those from previous epochs is done with caution, because relevant opacity effects may not be accounted for.

Although the interferometric phases for September 1993 contain key information about the emission asymmetry, the source was not large enough then for us to distinguish shell emission from disk emission even when we used the largest available Earth-sized array: A range of limb-brightened disk-like images, each with a characteristic size, are compatible with these data (image degeneracy) (4). Therefore, to determine the expansion rate without bias, we used the backward-extrapolated image from our November 1993 and May 1994 images in Fig. 1 in the mapping process to break this degeneracy and thus to estimate a size (4).

From observation in February 1994 we have high-quality data, but from only a three-antenna array. The interferometric amplitude data require a shell-like structure, and the interferometric phase data require an emission asymmetry in the shell. Use of a point-like source as an initial model made

J. M. Marcaide and E. Ros, Departamento de Astronomía, Universitat de València, E-46100 Burjassot, València, Spain.

A. Alberdi, Laboratorio de Astrofísica Espacial y Física Fundamental, Instituto Nacional de Técnica Aeroespacial (INTA), E-28080 Madrid, Spain, and Instituto de Astrofísica de Andalucía-Consejo Superior de Investigaciones Científicas (CSIC), Apdo. Correos 3004, E-18080 Granada, Spain.

P. Diamond, National Radio Astronomy Observatory, Socorro, NM 87801, USA.

I. I. Shapiro, Harvard-Smithsonian Center for Astrophysics, Cambridge, MA 02138, USA.

J. C. Guirado, D. L. Jones, R. A. Preston, Jet Propulsion Laboratory, California Institute of Technology, Pasadena, CA 91109, USA.

T. P. Krichbaum and A. Witzel, Max-Planck Institut für Radioastronomie, Auf dem Hügel 69, D-50131 Bonn, Germany.

F. Mantovani, Istituto di Radioastronomia, Consiglio Nazionale delle Ricerche (CNR), I-Bologna 40129, Italy.

A. Rius, Laboratorio de Astrofísica Espacial y Física Fundamental, INTA, E-28080 Madrid, Spain, and Centre d'Estudis Avançats-C.S.I.C., Camí de Santa Barbara s/n, E-17300 Blanes, Girona, Spain.

R. T. Schilizzi, Joint Institute for VLBI in Europe, Postbus 2, 7990 AA Dwingeloo, Netherlands, and Leiden Observatory, Postbus 9513, 2300 RA Leiden, Netherlands.

C. Trigilio, Istituto di Radioastronomia, CNR, Noto, Italy.

A. R. Whitney, Massachusetts Institute of Technology-Haystack Observatory, Westford, MA 01886, USA.

\*To whom correspondence should be addressed.

the imaging difficult. Instead, as an initial model we used a radio source that was similar to a map interpolated from those from November 1993 and May 1994 but was totally circularly symmetric. After only two mapping iterations, the image displayed the

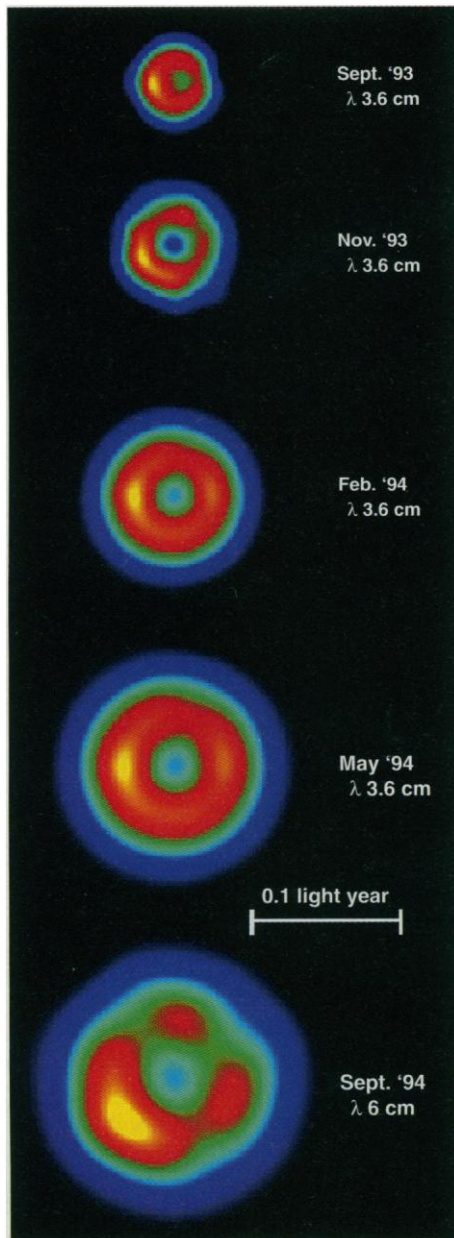


**Fig. 1.** Sequence of images of supernova SN 1993J made at the wavelengths ( $\lambda$ ) of 3.6 and 6 cm and placed at vertical positions proportional to days elapsed after explosion, clearly showing a uniform expansion. The images have been convolved by circular beams whose radii are proportional to the days elapsed after explosion, such that the two tangents to the images should converge to a point at explosion time. The sizes of the beams have been chosen to be within a factor of 2 of the interferometric beam of each observation. In the sequence of images, the extreme circular (spherical) symmetry of the expansion and the consistency of the emission enhancement in the southeast part of the shell-like emission are clearly apparent.

slight southeast emission enhancement characteristic of all the images.

The sequence of maps in Fig. 1 shows that the supernova expanded with circular symmetry. Hence, the asymmetry of the medium surrounding the progenitor and its reaction to the shock induced by the supernova ejecta must be small. In addition, the enhanced emission in the southeast survived but declined with time.

If we assume a free expansion similar to that indicated by older supernovae (5) and fit a straight line to the sizes measured at 3.6 cm and given in Table 1, with the constraint that the size is zero at the explosion date, we find an angular expansion rate of  $2.39 \pm 0.03 \mu\text{arcsec day}^{-1}$  (Fig. 2), which is very similar to our earlier estimate (1). Such an angular expansion rate corresponds, at the distance to SN 1993J of 3.6 Mpc (6), to an expansion speed of  $14,900 \pm 200 \text{ km s}^{-1}$ . If we fit to the 3.6-cm results a power law of the form  $\theta \propto t^m$ , where  $\theta$  is the angular radius,  $t$  the time after explosion, and  $m$  a deceleration parameter, we obtain  $m = 0.93 \pm 0.14$ . Size estimates reported even earlier (2, 3) appear to be biased toward higher values. Only if the radio supernova looked like a disk of uniform brightness at those earlier epochs rather than like a shell would those higher values correspond to true larger source sizes (4) and hence to higher early expansion speeds. If earlier estimates from Bartel *et al.* (3) were taken at face value, we

would obtain a deceleration with  $m = 0.82 \pm 0.03$ . In any case, the size estimate at 6 cm from the September 1994 data appears smaller than that expected from the 3.6-cm data only. Further images from later epochs at 6 cm are needed to help understand this surprising result.

All our maps show that the ratio of the shell thickness to the supernova shell outer radius is about 0.3 (7). Such a ratio and its (near) constancy are typical of self-similar models (8, 9) of emission generated in regions of circumstellar material shocked by supernova ejecta. To explain the slow rise of the early radio emission (10, 11), it has been argued that the density profile of the ionized circumstellar medium must be proportional to  $r^{-1.5}$ , where  $r$  is the distance from the supernova explosion center (11–14). Such a density profile is compatible with a disk-shaped density distribution seen edge-on (13, 14). From analyses of other aspects of the radio data it has also been argued that the circumstellar medium must have two mixed isotropic components, one smooth and one clumpy (11). The remarkable circular symmetry of all the images and the equally remarkable similarity of the 3.6- and 6-cm images imply a rather isotropic density distribution of the circumstellar medium.

In spite of our improved estimate of the expansion rate, based on the 3.6-cm data, the result does not imply a more accurate determination of the distance to M81 than

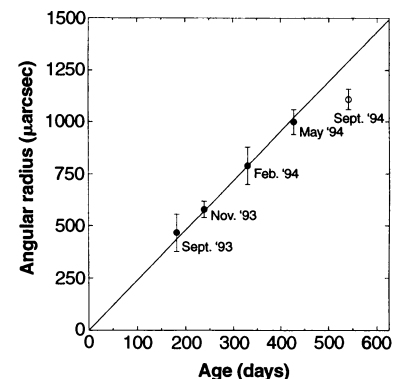
**Table 1.** SN 1993J observations and source parameters (30).

Date of observation	Age* (days)	Wave-length (cm)	Antenna symbol†	Total flux density used for mapping‡ (mJy)	Shell outer radius§ ( $\mu\text{arcsec}$ )
26 September 1993	182	3.6	BdLMY	78	$467 \pm 90$
22 November 1993	239	3.6	BDLMY	58	$581 \pm 40$
20 February 1994	330	3.6	DMY	51	$790 \pm 90$
29 May 1994	427	3.6	BDHLMNVY	42	$1000 \pm 60$
20 September 1994	541	6	BFHLNOTY	52	$1110 \pm 50$

\*Age of the supernova with respect to estimated explosion date of 28 March 1993. †See (30) for definitions. ‡Compact core of the galaxy M81 and compact source 0917 + 624 (31) used as calibrators. §Estimate from direct measurements on the images given in Fig. 1. See text and caption to Fig. 2.

†See (30) for definitions. ‡Compact core of the galaxy M81 and compact source 0917 + 624 (31) used as calibrators. §Estimate from direct measurements on the images given in Fig. 1. See text and caption to Fig. 2.

**Fig. 2.** Measured angular size (external radius of the shell) versus age of SN 1993J for observations made at 3.6 (solid circles) and 6 cm (open circle). The errors correspond to the root mean square (rms) of the radii measured along 24 cuts across the image equally spaced in azimuth. For February 1994 (day 330 after explosion), the error has been enlarged by a factor of 3 to account for the deficiency in the mapping as explained in the text; for a similar reason, the error for September 1993 (day 182) was arbitrarily made equal to that of February 1994, although this error corresponds for day 182 to 18 times the rms of the measured radii. The straight line through the origin is a weighted least-squares linear fit to the 3.6-cm data only, with the restriction that it must pass through the origin. It corresponds to an expansion rate of the outer shell radius of  $2.39 \mu\text{arcsec day}^{-1}$  ( $14,900 \pm 200 \text{ km s}^{-1}$  at an assumed distance of 3.6 Mpc).



obtained in earlier VLBI work (1) ( $3.8 \pm 0.8$  Mpc), because the uncertainty in the estimate of the maximum supernova ejecta speed by optical spectroscopy dominates. Recent spectra (15–17) show broad, flat-topped  $H\alpha$  emission from material moving at up to  $\sim 11,000$  km s $^{-1}$ . These speeds are much lower than those reported from early spectra (1, 3, 15, 18) and are about 30% lower than those we estimated for the outer shell radius if we assume a distance of 3.6 Mpc to M81 (6). However, because our estimate of the shell width is about 30% of the outer shell radius for every epoch of observation, the inner shell radius expands at  $\sim 70\%$  the rate of the outer radius. Such a coincidence is likely not accidental. Thus, the various estimates of the gas speeds are compatible, and there is no need to invoke any deceleration, if the highest speed  $H\alpha$  emission comes from around the reverse-shocked region just inside the innermost part of the radio shell (9, 12, 16, 19).

Chevalier and Blondin (20) have recently shown that the hydrodynamic instabilities generated by radiative cooling from the shocked region are not capable of producing the protrusions that have been observed in radio supernovae (21, 22). However, these authors also suggested that cases such as SN 1993J might have cooling reverse shocks capable of producing such protrusions, because the high level of radio emission is indicative of strong radiative cooling and of a dense circumstellar medium. Our images in Fig. 1, especially the one corresponding to May 1994, which is shown in Fig. 3 convolved with the full interferometric beam,

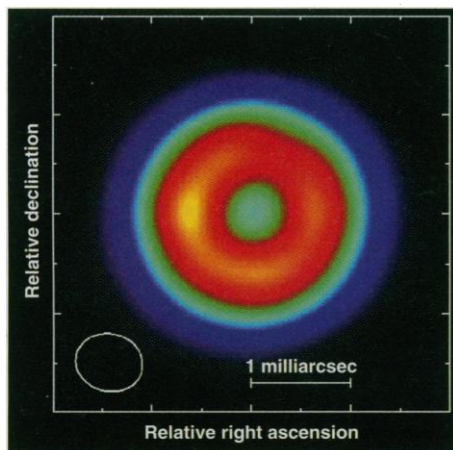


**Fig. 3.** Image at 3.6 cm (8.4 GHz) of SN 1993J from 29 May 1994, 427 days after explosion. The maximum brightness is 5.7 millijansky (mJy) per beam ( $1 \text{ Jy} = 10^{-26} \text{ W m}^{-2} \text{ Hz}^{-1}$ ). The elliptical gaussian beam used in the convolution to obtain this CLEAN map is shown in the lower left and has full widths at half maxima of  $0.68 \times 0.58$  milliarcsec, with the major axis along position angle  $77^\circ$ . One milliarcsecond is equivalent to  $5.4 \times 10^{16}$  cm (0.05 light year) for a distance to the supernova of 3.6 Mpc.

clearly show that SN 1993J does not yet have any protrusions. There is no evidence of instabilities having developed in any region of the source. The region of enhanced emission and the rest of the shell emission appear to evolve smoothly. Small changes in the position angle of emission features in the shell are not significant. These small differences are possibly due to imperfections in the imaging. Also, there is no clear evidence yet of deceleration of the supernova due to interaction with the circumstellar medium, and hence it may be too early to expect instabilities in the source due to convective or Rayleigh-Taylor instabilities (20).

The mechanism responsible for the enhanced emission in the southeast part of every image has to be capable of maintaining the enhancement over at least the 1-year period for which we have images. The region of enhanced emission appears in September 1994 as the region of steepest spectral index ( $\alpha \leq -1.5$ ,  $S \propto \nu^\alpha$ , where  $S$  denotes the flux density and  $\nu$  the frequency) of the source (average spectral index  $\alpha \sim -1.1$ ), which is perhaps indicative of a region with large energetic losses. From September 1993 to May 1994, the maximum brightness temperature in this region decreased from  $\sim 1.8 \times 10^9$  K to  $\sim 2.6 \times 10^8$  K (in the rest of the radio shell, such temperature decreased from  $\sim 1.1 \times 10^9$  K to  $\sim 2.0 \times 10^8$  K). It has been suggested (23, 24) that the progenitor was part of a binary system. The expansion rate of the supernova is such that the ejecta travel about 8 astronomical units per day. Hence, the ejecta would sweep past a putative close companion on a time scale of a day (24). It is perhaps conceivable that generation of local turbulence could in turn intensify the local energetics. The radio emission was first detected from SN 1993J 5 days after explosion (10). Until then, the radio emission was heavily absorbed at centimeter wavelengths, a condition persisting to a lesser degree at 3.6 cm through day 100 after explosion (11). Thus, although the interaction with a possible close companion would have taken place in the first days, its effects could not have been detectable for perhaps 2 or 3 months. Indeed, Bartel *et al.* (3) do not report any asymmetry in the emission from their VLBI observations during the first 60 days after explosion. What seems difficult to reconcile with the hypothesis that a companion star was the cause of the enhancement of emission is the large extent of the enhancement in November 1993, 8 months after explosion, and the survival of such an enhancement 12 months later.

There are other mechanisms that could enhance the emission (21) but would also produce a departure from circular symmetry, which has not been observed. Al-

though the circumstellar medium appears to be isotropic at the distances from the explosion point represented by the shell shown in our maps, it is conceivable that in the early stages of expansion the supernova ejecta encountered a circumstellar medium that was not quite isotropic, and hence radiation from the densest regions of the circumstellar medium could have increased. An anisotropic circumstellar medium close to the progenitor that was ionized by the initial supernova flash could also have given rise to the reported optical polarization (25). For this scenario to be plausible, a mechanism is needed to inhibit the alteration of the circular symmetry of the radio map by such a denser region. However, given that a variable stellar presupernova wind rate (11–14) has produced a circumstellar medium that has not detectably modified either the expansion rate or the circular symmetry, perhaps it is possible that a denser region of the circumstellar material had no other effect on the shock than to enhance the emission. Even the hypotheses of large-scale slightly anisotropic distribution of circumstellar material and of magnetic field density, with the relatively denser regions in the southeast directions being responsible for the enhanced radiation, are plausible.

#### REFERENCES AND NOTES

1. J. M. Marcaide *et al.*, *Nature* **373**, 44 (1995).
2. J. M. Marcaide *et al.*, *Astrophys. J.* **424**, L25 (1994).
3. N. Bartel *et al.*, *Nature* **368**, 610 (1994).
4. A. P. Marscher, in *Supernovae as Distance Indicators*, N. Bartel, Ed. (Springer, Berlin, 1985), pp. 130–137. The phase information from our September 1993 data requires an emission asymmetry in the image. This asymmetry is seen at later epochs as an emission enhancement in the southeast part of the otherwise circularly symmetric image.
5. T. W. B. Muxlow *et al.*, *Mon. Not. R. Astron. Soc.* **266**, 455 (1994).
6. W. L. Freedman *et al.*, *Astrophys. J.* **427**, 628 (1994).
7. We estimated this ratio by creating synthetic interferometric data corresponding to various shell models (4) and comparing the synthetic data with the data from the observations. Although the maps in Fig. 1 contain this information, it is not straightforward to obtain it from them only.
8. R. Chevalier, *Astrophys. J.* **259**, 302 (1982); *ibid.*, p. L85; *ibid.* **285**, L63 (1984); P. L. Biermann, in *Cosmic Winds and the Heliosphere*, J. R. Jokipii *et al.*, Eds. (Univ. of Arizona Press, Tucson, AZ, in press).
9. R. A. Chevalier and C. Fransson, *Astrophys. J.* **420**, 268 (1994). These authors have suggested a smaller extent for such a region, perhaps up to 15%, but Fransson (private communication) considers that widths of 30% are not ruled out by their models.
10. G. G. Pooley and D. A. Green, *Mon. Not. R. Astron. Soc.* **264**, L17 (1993); K. W. Weiler, S. D. Van Dyk, R. A. Sramek, N. Panagia, M. P. Rupen, in *Circumstellar Media in the Late Stages of Stellar Evolution*, R. E. S. Clegg, I. R. Stevens, W. P. S. Meikle, Eds. (Cambridge Univ. Press, Cambridge, 1994), pp. 207–212.
11. S. D. Van Dyk, K. W. Weiler, R. A. Sramek, M. P. Rupen, N. Panagia, *Astrophys. J.* **432**, L115 (1994).
12. C. Fransson, in *Circumstellar Media in the Late Stages of Stellar Evolution*, R. E. S. Clegg, I. R. Stevens, W. P. S. Meikle, Eds. (Cambridge Univ. Press, Cambridge, 1994), pp. 120–138.
13. P. Lundqvist, in *Circumstellar Media in the Late Stag-*

# Infrared Spectrum of the Cool Brown Dwarf Gl 229B

B. R. Oppenheimer, S. R. Kulkarni,\* K. Matthews, T. Nakajima

Spectroscopic measurements of a cool brown dwarf, Gl 229B, reveal absorption features attributable to methane in the near infrared much like those of Jupiter. These features are not seen in any star. The presence of methane indicates that the surface temperature of Gl 229B is below 1000 kelvin. Features attributed to water vapor also indicate that Gl 229B is much cooler than any known star.

Stars like our sun fuse hydrogen into helium and in the process produce energy, most of which appears as light. Current stellar models agree that objects less massive than  $0.08M_{\odot}$  cannot sustain hydrogen fusion (1, 2) (the sun is denoted by the symbol  $\odot$ , and  $M_{\odot}$  is the mass of the sun). Such objects are called brown dwarfs. When young ( $\approx 10^8$  years), they contract relatively rapidly, and the gravitational binding energy released makes these objects quite luminous. As they age, they rapidly cool, and grow dim, becoming increasingly harder to detect. At even lower masses, there exist giant planets, the only examples of which are the giant outer planets of our solar system, including Jupiter (mass  $M_J \sim 10^{-3} M_{\odot}$ ). According to theory, the objects in the mass range  $1M_J$  to  $100M_J$  have similar characteristics. All of them have fully convective interiors and thin radiative atmospheres that radiate mostly between bands of molecular absorption. In addition, they all have about the same radius,  $R \sim 0.1R_{\odot}$ . Despite these similarities, brown dwarfs and giant planets are thought to form differently. It is believed that planets condense within a protoplanetary disk. In contrast, brown dwarfs are thought to form like stars through direct condensations of interstellar gas.

There are at least two reasons why the study of brown dwarfs, especially cool brown dwarfs, excites considerable attention. First, astronomers would like to investigate these objects because they lie in the unexplored mass range between stars and planets. Although these objects were predicted some 30 years ago (1), the lack of unambiguous specimens has been a major stumbling block in this field. Second, planetary scientists would like to study the atmospheres of cool brown dwarfs to understand how they are related to the atmospheres of planets. Such understanding is critical in the search for other planetary systems.

The emergent spectrum of radiation from a condensed object depends on the chemical composition, the surface gravity,

and the effective surface temperature  $T_{\text{eff}}$  which is defined here by the relation  $\sigma T_{\text{eff}}^4 = L/4\pi R^2$ , where  $L$  is the luminosity of the object and  $\sigma$  is the Stefan-Boltzmann constant. The minimum luminosity of hydrogen-fusing stars (main-sequence stars) is  $10^{-4} L_{\odot}$  (2). Thus, for these stars,  $T_{\text{eff}} \approx 1800$  K. This is about equal to the temperature of GD 165B (3), the coolest condensed object known until the discovery of Gl 229B (4). As discussed above, old brown dwarfs do not generate nuclear power and thus can have very low  $T_{\text{eff}}$ .

At the low temperatures characteristic of planets and old brown dwarfs, molecules and possibly dust are readily formed. Molecules have a large number of energy levels, which drastically complicates detailed modeling of their atmospheres. To date, there exist no detailed models for  $T_{\text{eff}}$  below 2000 K (5, 6). However, predictions do exist. For example, below  $T_{\text{eff}}$  of 1000 K, most of the carbon is predicted (7) to reside in methane ( $\text{CH}_4$ ). In contrast, the cool, late-type stars (with  $T_{\text{eff}} > 1800$  K) have no  $\text{CH}_4$ . Their carbon resides mainly in CO, which has a distinctive appearance in spectra of these stars.

Observations of cool objects are crucial to any further progress in this field. As Stevenson (8) remarked in a review of high-mass planets and brown dwarfs, "The biggest challenges for the future lie not in theory but in observations: we need more than two colors. We need spectra. . . . Refinement of the theory does not seem to be a compelling task until this happens."

Here we report the first near-infrared (IR) spectroscopic observation of a cool brown dwarf, Gl 229B (4). This object has the same proper motion as that of Gl 229 and is thus most likely a companion of Gl 229 (hereafter Gl 229A). Nakajima *et al.* (4) obtained broadband photometric measurements from which they deduced  $L \leq 10^{-5} L_{\odot}$ . This is 1/10 of the minimum luminosity of any main-sequence star. Nakajima *et al.* concluded that Gl 229B is a cool ( $T_{\text{eff}} \leq 1200$  K) condensed object. At the present time, we are unable to determine the origin of this object. For simplicity, we will refer to Gl 229B as a brown dwarf.

Palomar Observatory 105-24, California Institute of Technology, Pasadena, CA 91125, USA.

\*To whom correspondence should be addressed.

- es of Stellar Evolution*, R. E. S. Clegg, I. R. Stevens, W. P. S. Meikle, Eds. (Cambridge Univ. Press, Cambridge, 1994), pp. 213–220.
14. C. Fransson, P. Lundqvist, R. A. Chevalier, *Astrophys. J.*, in press.
  15. A. V. Filippenko, T. Matheson, A. J. Barth, *Astron. J.* **108**, 2220 (1994).
  16. F. Patat, N. Chugai, P. A. Mazzali, *Astron. Astrophys.* **299**, 715 (1995).
  17. The maximum velocity estimate was obtained from the red side of the  $\text{H}\alpha$  emission because the blue side appears blended with emission from neutral oxygen [OI]. Even more recent spectra (29) that are free of [OI] emission also show a symmetrical flat-topped  $\text{H}\alpha$  emission centered at  $6560 \text{ \AA}$ , with gas speeds also having maxima with similar values.
  18. J. R. Lewis *et al.*, *Mon. Not. R. Astron. Soc.* **266**, L27 (1994).
  19. R. Terlevich, G. Tenorio-Tagle, J. Franco, J. Melnick, *ibid.* **255**, 713 (1992). The highest speed  $\text{H}\alpha$  emission would originate at the cool shell outward of the reverse-shocked region and at the outermost part of the ejecta close to the reverse shock.
  20. R. A. Chevalier and J. M. Blondin, *Astrophys. J.* **444**, 312 (1995).
  21. N. Bartel *et al.*, *ibid.* **323**, 505 (1987).
  22. N. Bartel *et al.*, *Nature* **350**, 212 (1991).
  23. K. Nomoto *et al.*, *ibid.* **364**, 507 (1993); Ph. Podsiadlowski *et al.*, *ibid.*, p. 509.
  24. S. E. Woosley *et al.*, *Astrophys. J.* **429**, 300 (1994).
  25. S. R. Trammell *et al.*, *ibid.* **414**, L21 (1993).
  26. A. E. E. Rogers *et al.*, *Science* **219**, 51 (1983).
  27. J. D. Romney, in *The Impact of VLBI on Astrophysics and Geophysics*, M. Reid and J. M. Moran, Eds. (Kluwer, Dordrecht, Netherlands, 1988), pp. 461–468.
  28. T. J. Pearson, *Bull. Am. Astron. Soc.* **23**, 991 (1991).
  29. C. Fransson, private communication; A. V. Filippenko, private communication.
  30. The observations were made with the following antennas (symbols, diameters, affiliations, and locations are given in parentheses): Effelsberg (E, 100 m, Max-Planck Institut für Radioastronomie (MPIfR), Effelsberg, Germany); DSS15 (d, 34 m, NASA, Goldstone, CA); DSS14 (D, 70 m, NASA, Goldstone, CA); Fort Davis (F, 25 m, Fort Davis, TX); Hancock (H, 25 m, Hancock, NH); Medicina (L, 32 m, CNR, Medicina, Italy); DSS63 (M, 70 m, NASA, Robledo, Spain); Noto (N, 32 m, CNR, Noto, Italy); Owens Valley (O, 25 m, Big Pine, CA); Kitt Peak (T, 25 m, Kitt Peak, AZ); Saint Croix (V, 25 m, U.S. Virgin Islands); VLA [Y, equivalent diameter 130 m, National Radio Astronomy Observatory (NRAO), near Socorro, NM]. At each station, a hydrogen maser frequency standard was used to govern the local oscillator chain and the "time tagging" of the recorded data. The data were recorded with the Mark IIIA (26) or compatible very long baseline array (VLBA) instrumentation (27), in mode B double speed, yielding bandwidths of 56 MHz. Right-hand circular polarization (IEEE convention) was recorded at the wavelength of 3.6 cm, and left-hand circular polarization was recorded at 6 cm. The data were correlated at MPIfR, Bonn, Germany and were further analyzed with the Caltech VLBI Package (28).
  31. K. J. Standke *et al.*, *Astron. Astrophys.*, in press.
  32. We thank the many people that made this research possible: B. Clark, R. Schwartz, P. Wolken, and the staffs at the participating observatories, at NASA-JPL, and at the MPIfR, where all the data were correlated. We also thank K. W. Weiler for useful comments on our manuscript. This research was partly supported by the Dirección General de Investigación Científica y Tecnológica in Spain and by NSF in the United States. NRAO is a facility of NSF operated under cooperative agreement by Associated Universities, Inc. DSS14, DSS15, and DSS63 are operated by NASA-JPL. This work was carried out in part by JPL, California Institute of Technology, under contract to NASA. E.R. acknowledges receipt of a scholarship of the Generalitat-Valenciana. Partial support for the correlator operation from the European Union Access to Large Scale Facilities Programme is acknowledged.

2 August 1995; accepted 10 October 1995